Received: 4 January 2022 | Revised: 27 March 2022 | Accepted: 31 March 2022

DOI: 10.1111/ppl.13682

SPECIAL ISSUE ARTICLE

Physiologia Plantarum

Oxygen uptake rates have contrasting responses to temperature in the root meristem and elongation zone

Maura J. Zimmermann[1,2] | Jayakumar Bose[3] | Eric M. Kramer[4] | Owen K. Atkin[5] | Stephen D. Tyerman[3] | Tobias I. Baskin[2]

[1]Plant Biology Program, University of Massachusetts, Amherst, Massachusetts, USA

[2]Biology Department, University of Massachusetts, Amherst, Massachusetts, USA

[3]School of Agriculture, Food and Wine, Australian Research Council Centre of Excellence in Plant Energy Biology, University of Adelaide, Glen Osmond, South Australia, Australia

[4]Physics Department, Bard College at Simon's Rock, Great Barrington, Massachusetts, USA

[5]ARC Centre of Excellence in Plant Energy Biology, Research School of Biology, The Australian National University, Canberra, Australian Capital Territory, Australia

Correspondence
Tobias I. Baskin, Biology Department, University of Massachusetts, Amherst, MA, USA.
Email: baskin@umass.edu

Funding information
United States National Science Foundation, Grant/Award Number: IOS - 2035814; Australian Research Council, Grant/Award Number: CE140100008

Edited by: R.E. Sharp

Abstract

Growing at either 15 or 25°C, roots of *Arabidopsis thaliana*, Columbia accession, produce cells at the same rate and have growth zones of the same length. To determine whether this constancy is related to energetics, we measured oxygen uptake by means of a vibrating oxygen-selective electrode. Concomitantly, the spatial distribution of elongation was measured kinematically, delineating meristem and elongation zone. All seedlings were germinated, grown, and measured at a given temperature (15 or 25°C). Columbia was compared to lines where cell production rate roughly doubles between 15 and 25°C: Landsberg and two Columbia mutants, *er-105* and *ahk3-3*. For all genotypes and temperatures, oxygen uptake rate at any position was highest at the root cap, where mitochondrial density was maximal, based on the fluorescence of a reporter. Uptake rate declined through the meristem to plateau within the elongation zone. For oxygen uptake rate integrated over a zone, the meristem had steady-state Q_{10} values ranging from 0.7 to 2.1; by contrast, the elongation zone had values ranging from 2.6 to 3.3, implying that this zone exerts a greater respiratory demand. These results highlight a substantial energy consumption by the root cap, perhaps helpful for maintaining hypoxia in stem cells, and suggest that rapid elongation is metabolically more costly than is cell division.

1 | INTRODUCTION

Plants, like all organisms, are challenged by fluctuating temperatures. A rise in thermal energy accelerates every molecule, potentially sundering finely tuned metabolic pathways. An animal can meet this challenge by moving to a new location or by pumping a fluid through its body to exchange and ultimately remove heat. For plants, these strategies are largely unavailable, although plants do move their leaves and transpire water, both processes offering some relief from temperature fluctuations. Instead, plants meet the challenge of changes in temperature mainly through metabolic acclimation. In this process, the plant copes with temperature changes by adjusting the rates of specific pathways or activities.

Typically, processes such as growth or respiration speed up with temperature over the short term, reflecting direct effects of temperature on enzyme activity and indirect effects on the demand for respiratory energy (Atkin et al., 2000). This relationship between temperature and respiration happens in ectothermic organisms ranging from plants (Lambers et al., 2008) to scorpions (van Aardt et al., 2016). When a plant is first exposed to a temperature increase, rates of growth or respiration may double for a 10°C rise (i.e., Q_{10} equals 2). However, with sustained warming, growth or respiratory metabolism often acclimates, as seen by their rates being lower in warm-acclimated plants than in cold-acclimated ones when measured at a common temperature (Armstrong et al., 2006; Loveys et al., 2003). In fact, acclimation can reach homeostasis, as seen by cold- and warm-grown plants growing or respiring at similar rates,

even when measured at their respective growth temperature (Atkin et al., 2005; Larigauderie & Körner, 1995; Loveys et al., 2002). Whether or not reaching homeostasis, rates of growth and respiration change with temperature based on energy demand from processes such as protein turnover, transport across membranes, and oxidative phosphorylation (Amthor, 1984; Atkin et al., 2000; Huang et al., 2012; Scafaro et al., 2021; Scheurwater et al., 1998; van der Werf et al., 1988).

Our understanding of how growth and respiration acclimate to temperature in plants is reasonably advanced; nevertheless, much of the work is integrative, carried out at the level of the whole plant or organ. For example, root respiration is commonly measured for a soil container encapsulating the whole root system (Bouma et al., 1997) or for detached root systems or segments placed in an aerated solution (Loveys et al., 2003). Likewise, growth is widely taken as relative gain of dry weight of the organ (or plant), thereby integrating the activity of expanding and non-expanding cells. Expanding cells make a relatively thin, primary cell wall and may also divide; non-expanding cells synthesize a secondary cell wall, which is massive in many cell types, and they may synthesize copious amounts of secondary metabolites. Although expanding leaves have a greater respiratory demand than mature ones (Armstrong et al., 2006), the respiratory demands exerted specifically by expanding cells have rarely been evaluated in response to temperature. Consequently, we do not know to what extent growth processes in expanding and non-expanding cells involve distinct relationships between temperature and respiration.

The growth processes of expanding cells plausibly place unique demands on respiratory metabolism. Cells in the meristem replicate their contents over a cell cycle (typically 10–20 h, Grif et al., 2002), a sustained synthetic activity that might need a particularly plentiful supply of adenosine triphosphate (ATP) and reducing equivalents (Amthor et al., 2019). For expansion, water uptake is driven by a large osmotic gradient, which plausibly exerts a large energy demand (Fricke, 2017). Ion uptake has long been recognized as having a substantial respiratory cost (Poorter et al., 1991; van der Werf et al., 1988), although cost was not tied explicitly to expansive growth.

For several reasons, energy demands of expansive growth are likely to be acute for roots. In the root, the carbon compounds needed for energy and biosynthesis must be imported from the shoot, requiring extra machinery for partitioning (Ross-Elliott et al., 2017). Growing root cells, in addition to satisfying their own metabolic needs, secrete organic material into the rhizosphere; the amount secreted is appreciable, amounting to as much as a quarter of the carbon imported (Vives-Peris et al., 2020). In the root elongation zone, cells have relative expansion rates that are typically 5–10 times greater than those of shoots (Silk, 1984), and yet maintain a relatively constant cell wall thickness (Jensen & Ashton, 1960), a high-octane performance that is plausibly associated with high metabolic demand. Without characterizing the energy demands of primary growth processes specifically, our understanding of thermal respiratory acclimation of developing roots will remain incomplete.

That expansive growth demands considerable energy is perhaps consistent with some studies showing that rates of respiration are maximal at the root tip and decrease toward the shoot (Bingham et al., 1996; Darwent et al., 2003; Luxmoore et al., 1970; Norris Jr. et al., 1959). But in other studies, respiration rates are more or less uniform along the root (Stepniewski et al., 1998) or vary with position in a complex way (Bidel et al., 2001). However, in all these studies, the "tip" lumps meristem, elongation zone, and part of the adjacent mature zone.

More recently, measurements with finer spatial resolution became possible with the advent of the vibrating, oxygen-selective electrode (Newman, 2001; Pandolfi et al., 2012). By vibrating toward and away from the root, the electrode experiences oxygen concentration at two positions: one near, the other farther from the root surface. This difference, along with the distance between probe measurements, enables the rate of oxygen uptake to be estimated. This technique assumes that, within an unstirred boundary layer extending from the root surface into the bulk solution, metabolic activity establishes a steady-state gradient of oxygen. A stable gradient is established by an equilibrium between the rate of oxygen removal in tissues and resupply by diffusion from the bulk medium. The gradient drives a flux of oxygen into the root and thus, by measuring the external flux, we can infer the internal rate of oxygen consumption. Along the root axis, the vibrating probe has a spatial resolution in the tens of microns, allowing oxygen uptake to be measured as a function of position, easily resolving meristem and elongation zone.

As with the studies mentioned above, for oxygen uptake measured by a vibrating probe, the rate is usually greatest at the root tip (e.g., McLamore et al., 2010; Mugnai et al., 2012). In these studies, given their spatial resolution, "the tip" probably means the root cap, although anatomical data were not presented. However, along with respiration, elongation was rarely measured concomitantly; thus, it is difficult to relate the reported uptake to specific zones in the root or even to know if the roots were elongating during measurement. Furthermore, measurements of oxygen uptake in intact roots as a function of temperature have, to our knowledge, never been reported with a spatial resolution sufficient to discriminate contributions from meristem and elongation zone. Therefore, our knowledge about respiratory acclimation to temperature in dividing or rapidly elongating cells is mainly speculative.

Here, by means of the vibrating probe, we quantified oxygen uptake as a function of temperature within the root meristem and elongation zone. For this work, we used *Arabidopsis thaliana* because the small size of these roots facilitates measuring growth and respiration and because the powerful community resources for this species allow discoveries to be translated effectively to farm and field (e.g., Borrill, 2020; https://www.arabidopsis.org). Concomitantly, we quantified the spatial profile of elongation (Baskin, 2013; Silk, 1984), allowing meristem and elongation zone to be delineated functionally. Elongation and oxygen uptake were measured on the same roots at essentially the same time.

For these experiments, seedlings were germinated and grown continuously at either 15 or 25°C and then assayed at their growth temperature. This contrasts with the more typical approach where

material is grown at one temperature or another and then shifted to a common temperature for measurement. The common temperature provides a consistent reference; however, during measurement, the plants might be responding to the new temperature. Here, such responses could well be problematic because collecting vibrating probe data for a single root required about 1 h, a time long enough for the new temperature to elicit responses. By using continuous conditions, we compare steady-state performance (Larigauderie & Körner, 1995).

We built on previous work showing that, in the Columbia accession of *A. thaliana* roots, certain cell division and elongation activities occur at similar rates despite growth at different temperatures, i.e. they are homeostatic (Yang et al., 2017). Specifically, comparing plants grown and assayed at 15 and 25°C, the meristem produces cells at essentially the same rate and the growth zone (i.e., meristem plus elongation zone) spans the same length. Intuitively one might expect cells to be produced faster at 25 than at 15°C and the root to have a larger growth zone. Indeed, a wide variety of plant developmental processes are faster at 25 than 15°C (Parent and Tardieu, 2012). We hypothesized that the thermal homeostasis observed by Yang et al. (2017) for cell production rate and growth zone length is underpinned by increased energy demand in the 15°C-grown plants relative to their 25°C counterparts, a demand that would be reflected by respiration rates. For example, rates at 15°C might be unexpectedly high.

To test the hypothesis that cell production and elongation are metabolically costly, we compared the Columbia accession, in which, as described above, cell production rate and growth zone length are homeostatic (Yang et al., 2017), not only to another accession (Landsberg *erecta*), but also to two Columbia mutants, (*ahk3-3* and *er-105*), in all of which preliminary observations indicated that cell production rate is not homeostatic across a range of growth temperatures. Taken together, our results tend to refute the hypothesis for division and support it for elongation, although it is not clear whether costs arise from the elongation process itself or from maintaining a cell with a giant vacuole. Interestingly, the major consumer of oxygen per unit length appears to be the root cap.

2 | MATERIALS AND METHODS

2.1 | Plant growth conditions

A. thaliana (L.) Heynh seeds were stored at 4°C. On day 0, they were surface sterilized in 15% bleach and rinsed 5 times in sterile water. Seeds were sown on growth medium (modified Hoagland's solution supplemented with 1% sucrose; Baskin & Wilson, 1997) solidified with 0.9% agar in 10 cm × 10 cm square plates and grown axenically. For experiments with Columbia or Landsberg *erecta*, there were 10 seedlings per plate, with three plates per temperature; with *ahk3-3* and *er-105*, there were six mutant seedlings on one side of the plate and six of the wild type (Columbia) on the other side, again with three plates per temperature.

Except for studies of mitochondrial density (see below), experiments were done at the University of Adelaide, Australia. Plates were placed in a growth chamber (Adaptis CMP6010, Conviron, Urrbrae Australia) with a constant light intensity of approximately 80 μmol m^{-2} s^{-1} at either 15 or 25°C. Humidity within the chamber was set to 80%. Assays were started when plants grown at 25°C were 7-days old (with roots around 7 cm in length) and when those grown at 15°C were 14-days old (~4 cm roots), times when root elongation rate becomes roughly constant (Yang et al., 2017). Oxygen uptake and the spatial profile of growth were measured on the same plants; whereas, cell production rate was measured either the day before or the day after oxygen uptake measurements, but on distinct plants. Oxygen uptake was measured over the course of 3–4 days for each genotype, taking care to use plants of the same age (batches of seeds were plated every day to ensure a supply). New plants were used each day, so that plates that had been opened previously were not used. To keep plates at the same temperature during transport to the oxygen microelectrodes, they were placed in a cooler with an aluminum plate heated or cooled to the growth temperature (15 or 25°C).

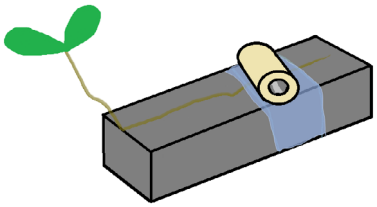

FIGURE 1 A schematic of the assembly used to immobilize the root. The root was affixed to a plastic brick (gray block) via Parafilm (blue), both were kept from moving by placing a little rubber stopper on them (yellow). The assembly was placed in a chamber and the root submerged 14 mm below the surface for experiments

2.2 | Cell production rate assay

Cell production rate was calculated for each root by dividing the average mature cell length by root growth rate (Baskin, 2013). To measure root growth rate, the back of the plate was scored at the position of the root tip, once a day, including the last day of the experiment, at which time the plate was scanned. Then, the length of the root between score marks was measured (ImageJ, Schneider et al., 2012) and divided by the time interval between marking. After scanning, the root was cut at the penultimate score mark and the excised segment (which contains the tip and cells made during the preceding 24 h) was imaged through a compound microscope with a ×20 objective lens and Nomarski optics. For each root, the lengths of 25 mature cortical cells were measured starting where root hairs are fully grown.

2.3 | Oxygen uptake measurements

Seedlings were removed from the agar and affixed with pre-stretched Parafilm to a plastic brick, which prevented the root from moving when submerged (Figure 1). Approximately 20 μL of well-oxygenated,

sterile growth medium, pre-equilibrated to the measuring temperature (either 15 or 25°C, the same temperature as used for seedling growth) was placed on the brick prior to attaching the root, to minimize drying while the root was attached. Immediately after attaching the root, the assembly was placed in a chamber (65 mm long, 5 mm wide, and 20 mm high) filled with ~5 mL of the same growth medium. The root was ~14 mm from the surface and the shoot was not submerged. To ensure the brick (and by extension the root) did not move within the chamber, a stopper was placed on top of the brick. Then, the chamber was attached to a three-dimensional micromanipulator (Xiao et al., 2018). Measurements were taken along the apical ~2 mm of the root.

To maintain constant temperature during the experiment, two sides of the chamber were held in close contact with thin copper pipes, which were connected via plastic tubing to a circulating, temperature-controlled water bath. The temperature of the medium was monitored throughout the experiment by using an infrared thermometer (Fluke 568, Fluke Australia Pty Ltd, NSW, Australia) and a thermocouple inserted into the growth medium. Temperature was kept steady at 15 or 25 ± 0.4°C.

Root oxygen uptake was measured by using a Clark-type oxygen microelectrode with a tip diameter of 25 μm (OX-25; Unisense A/S, Aarhus, Denmark). The microelectrode was calibrated via a two-point calibration by using an oxygenated solution (aerated Milli-Q water containing 272 μmol O_2 L^{-1} at 22°C) and an oxygen-free solution (0.1 M NaOH, 0.1 M $C_6H_7NaO_6$), each at measurement temperature (Xiao et al., 2018). The probe was calibrated prior to each measurement session.

After calibration, the electrode was carefully placed in a clamp on a micromanipulator that allowed for three-dimensional positioning. This was attached to a motor, which was controlled by Sensor Trace PRO (Version 3.2.8; Unisense A/S). The motor allowed for the probe to be moved toward or away from the root surface, but movement parallel to the root's long axis was done manually via the micromanipulator. The electrode was placed ~76 μm away from the root surface and aligned with the root by putting them in the same focal plane. Approximately 3 min after submerging the root, oxygen probe measurements started, usually at the position of the quiescent center of the root (Figure 5), estimated visually. The root was moved 76 μm between uptake measurements to 456 μm from the quiescent center (at or beyond the start of the elongation zone) and 156 μm thereafter, until the mature zone was reached, which was defined by well emerged root hairs.

At each position, six measurements were taken over a 10 s interval, then later averaged. Each measurement comprised data from close to and far from the surface of the root (76 and 250 μm, respectively). The six raw data points per position revealed no consistent trends (e.g., steady increase or decrease) implying that oxygen uptake was stable over this time scale. After moving to a new position, 3 s elapsed before recording data to minimize transients from the chamber motion.

A full set of uptake measurements typically took at least 1 h. However, during that hour the root responds to gravity and might respond to submergence. To see if either impacted measured rates of oxygen uptake, for at least three roots per genotype, the probe was placed 360 μm away from the root tip, moved shootward in increments of 152 μm until the mature zone was reached, then moved back to the quiescent center for the final measurements. Although not analyzed rigorously, data obtained in this manner appeared similar to data obtained as described above, again suggesting that the oxygen uptake profiles were reasonably stable over the hour.

2.4 | Oxygen uptake rate calculations

We relate concentration gradients measured outside the root to the radial oxygen flux at the root surface (i.e., uptake) by following the technique described in Henriksen et al. (1992). For a cylindrical root of infinite length and radius r_o,

$$J = \frac{uRT\,(C_2 - C_1)}{r_o \ln (r_2/r_1)} \quad (1)$$

where J is the flux at the root surface (reported here as *oxygen uptake rate*), u is the mobility of oxygen in the medium (9.13×10^{-13} mol m s^{-1} N^{-1}; corrected from Pang et al., 2006) essentially constant between 15 and 25°C, R is the gas constant, T is temperature, C_i is the concentration of oxygen, and r_i is the radial distance from the center of the root to the position of measurement. For C_i and r_i, the subscript denotes the measurement position. Here, $r_1 = r_o + 76$ μm and $r_2 = r_1 + 250$ μm. Concentrations were obtained from the electrode's voltage output as described above.

2.5 | Modeling oxygen concentration for a tapered root

To evaluate the consequences of the root's tapering and finite length for flux data calculated from Equation (1), which assumes a right cylinder of infinite length, we modeled the root as consuming oxygen uniformly per unit volume throughout its length. We approximate the root volume as a cylinder of radius R_{cyl} and length L_{cyl}, with an additional parabolic tip of length L_{tip}. Setting the model root apex at the origin, with the z-axis being the long axis of the root, and using cylindrical coordinates (ρ, z), our approximation for the root profile is:

$$\rho(z) = \begin{cases} R_{cyl}\,(z/L_{tip})^{1/2} & 0 \le z \le L_{tip} \\ R_{cyl} & L_{tip} \le z \le L_{tot} \end{cases} \quad (2)$$

where L_{tot} is the total root length, the sum of the lengths of the cylindrical and parabolic pieces, $L_{tot} = L_{tip} + L_{cyl}$. These equations fitted the measured radial profile of the root well. Based on the fits, we selected $L_{tip} = 272$ μm. The total length of the model root must be large compared to the zone of flux measurements, but is otherwise arbitrary, hence $L_{cyl} = 5.0$ cm.

If (as modeled) oxygen consumption per unit volume is constant, then oxygen consumption is proportional to the cross-sectional area, πR^2. Oxygen consumption σ_{cyl} in the cylindrical portion of the model root is therefore constant and, in the parabolic tip, it decreases linearly from σ_{cyl} to 0 at the apex. The consumption along the model root is thus:

$$\sigma(z) = \begin{cases} \sigma_{cyl}(z/L_{tip}) & 0 \le z \le L_{tip} \\ \sigma_{cyl} & L_{tip} \le z \le L_{tot} \end{cases} \quad (3)$$

Exterior to the root, the steady-state concentration of oxygen $C(\mathbf{r})$ satisfies the Laplace equation, $\nabla^2 C = 0$. Therefore, because the electrostatic potential also satisfies the Laplace equation, the mathematical form of C can be found using techniques developed for the electrostatic potential of a line charge (Andrews, 1997). Since we are only interested in the concentration outside the root, the detailed distribution of oxygen sinks inside the root may be modeled by approximating the entire sink strength, Equation (3), as a linear distribution on the z-axis. The solution for the steady-state concentration outside the root may then be written:

$$C(\rho,z) = -A(f_1(\rho,z) + f_2(\rho,z)) \quad (4)$$

where A is a multiplicative constant, the term f_1 is due to the presence of the tapered sink between $z = 0$ and $z = L_{tip}$ (see Equation 3), and the term f_2 is due to the presence of a constant linear sink of strength σ_{cyl} between $z = L_{tip}$ and $z = L_{tot}$. The two functions f are:

$$f_1(\rho z) = \left\{ -\sqrt{z^2+\rho^2} + \sqrt{(L_{tip}-z)^2+\rho^2} + z\, ln\left[\frac{(L_{tip}-z) + \sqrt{(L_{tip}-z)^2+\rho^2}}{-z+\sqrt{z^2+\rho^2}} \right] \right\} \frac{1}{L_{tip}} \quad (5)$$

$$f_2(\rho z) = ln\left[\frac{(L_{tot}-z) + \sqrt{(L_{tot}-z)^2+\rho^2}}{(L_{tip}-z) + \sqrt{(L_{tip}-z)^2+\rho^2}} \right]$$

Equation (5) was rederived and simplified from the expressions in Andrews (1997) by using the symbolic calculator, Maple (Waterloo Maple, version 2020.2).

2.6 | Physical model of a tapering root

An artificial tapering root was made from yeast embedded in agarose. The wine yeast (*Saccharomyces bayanus*, Lalvin EC 1118, population density more than 10^{10} UFC/g) was grown in yeast-extract peptone dextrose (YPD) medium and then mixed with melted agarose in the same medium for a final concentration of 1% (w/v) agarose. Prior to gelling, the yeast-agarose mixture was loaded into specially fabricated micro-capillaries, made by pulling non-filamentous borosilicate glass capillaries (GC 150-10, internal diameter 0.86 mm, Harvard Apparatus Ltd) to less than 1 μm tip diameter on a vertical puller (PP830, Narishige), and then breaking the tip to form a ~300 μm opening. Once cooled, gentle pressure applied by a syringe expelled the yeast-embedded agarose "root" into a solution of 5 mM glucose. The artificial root was immobilized on a plastic brick by using stretched Parafilm strip and incubated in the medium for 30 min. Then oxygen flux measurements were performed as for real roots.

2.7 | Spatial profile of growth

Concomitantly with measuring oxygen uptake, the submerged root in the chamber was imaged through a microscope connected to a camera (LCMOS-09000-KPB; Industrial Digital Camera) controlled by software (Optipix ImageView). The display was also used to guide translocation of the root between uptake measurements. Image sequences were acquired before uptake measurement began (0 min), in the middle of measurements (20–30 min), and after (50–60 min). At 15°C, image sequences were taken for 120 s, with 10 s between images. At 25°C, images were taken for 100 s with 10 s between images.

The spatial profile of velocity was obtained by Stripflow, software described previously (Baskin & Zelinsky, 2019; Yang et al., 2017). Briefly, the program uses a pair of images and finds the velocity parallel to the root's midline at each point of that midline. Here, we obtained velocity profiles from images separated by 30 s and averaged three profiles to reduce noise. Because images were acquired at 10 s intervals, this amounts to a total elapsed time of 50 s. Velocity profiles were fitted to a modified logistic function that has parameters identifying the length of the elongation zone and the relative elongation rate within that zone (Peters & Baskin, 2006). For some roots, a velocity profile was unattainable because the roots grew toward or away from the camera.

2.8 | Spatial profile of mitochondrial density

Mitochondrial density was characterized at UMass Amherst. Seeds of a line in the Columbia background that expresses yellow fluorescent protein (YFP) targeted to mitochondria by means of a 29 amino-acid signal sequence (mt-yk CS16264; Nelson et al., 2007) were handled as described above, except that they were grown in a Percival growth chamber (CU36L5; Perry, IA) with a constant light intensity of approximately 70 μmol m^{-2} s^{-1} and without humidity control. Seedlings were grown for 7 days at 25°C and 14 days at 15°C. Roots were excised and mounted in 0.01% Trition and imaged through a 10× objective on a spinning disk confocal microscope (3i; https://www.intelligent-imaging.com) equipped with a Yokagawa W1 spinning disk and an iXon Life 888 EM-CCD camera (Andor; https://andor.oxinst.com). YFP fluorescence was excited by 514-nm 100 mW solid state laser with a 542/27 emission filter. Overlapping stacks were acquired spanning the apical 3 mm of the root.

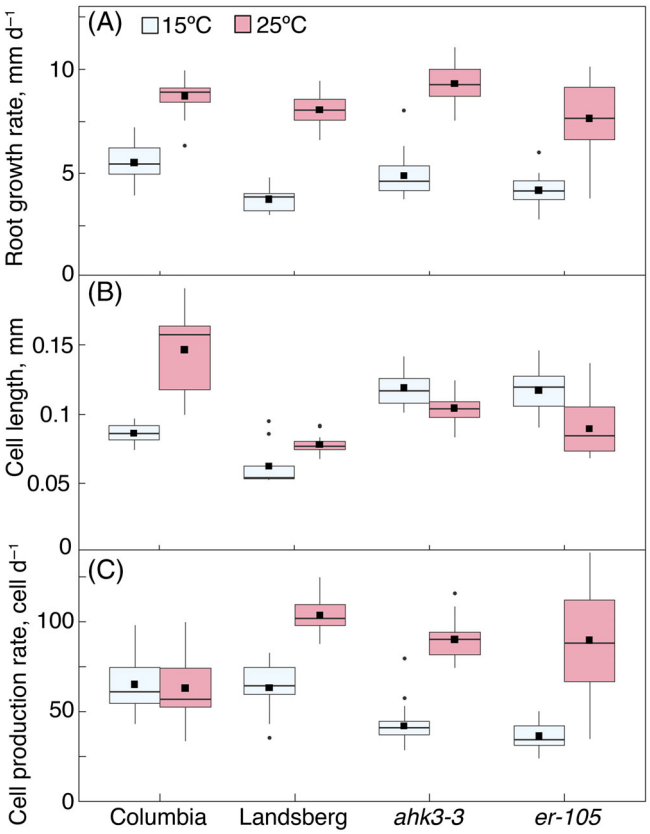

FIGURE 2 Growth parameters for roots grown on plates. The square symbol shows the mean, while the box and whiskers show the data distribution, the horizontal black lines are the median, and the dots are outliers. (A) Root elongation rate over the 24 h preceding cell length measurement. (B) Cell length. Fully mature cortical cells were measured that were produced over the previous day. (C) Cell production rate, the ratio of root growth rate to cell length. Each temperature had approximately 20 seedlings measured per genotype

From each stack, the approximately median optical section was selected and mosaiced together. Then, average intensity was measured along a 26 μm wide strip following the edge of the root (ImageJ). Strips were measured along the two sides of the root and averaged.

3 | RESULTS

3.1 | Temperature acclimation of cell production rate

As described in Section 1, the root meristem of the Columbia accession of *A. thaliana* was reported to have a surprising thermal acclimation; specifically, the same rate of cell production for seedlings grown and measured at either 15 or 25°C (Yang et al., 2017). Before testing our hypothesis that this acclimation reflects the costliness of division, we determined whether the report was reproducible. For roots growing at steady state, cell production rate equals the ratio of root growth rate to mature cell length (Baskin, 2013; Silk et al., 1989). For this calculation, we measure cortical cells because they are large and easy to delineate; therefore, the cell production rate obtained applies strictly to the cortex, but we assume the rate of cell production in this tissue is representative of other tissues. Confirming the previous report, while root growth rate and cell length nearly doubled for Columbia grown at 25°C compared to seedlings grown at 15°C, cell production rate was indistinguishable (Figure 2).

We also examined three other genotypes, namely: the Landsberg *erecta* (Ler) accession and two mutants in the Columbia background: *ahk3-3* and *er-105*. AHK3 is a histidine kinase mediating responses to cytokinin (Riefler et al., 2006). The *er-105* line has a null mutation in the erecta kinase (Torii et al., 1996), thereby allowing phenotypes caused by the missing kinase to be distinguished from those caused by the genetic background (i.e., Landsberg). Notably, the erecta kinase has been linked to responses to temperature of the shoot (Patel et al., 2013; Qi et al., 2004; Shen et al., 2015). In all three genotypes, root growth and cell production rate at 25°C were roughly twice their values at 15°C (Figure 2), showing that in these lines, in contrast to Columbia, cell production rate does not acclimate.

3.2 | Oxygen uptake as a function of position and temperature

To characterize oxygen uptake as a function of position, we used a vibrating probe with an oxygen selective electrode (Xiao et al., 2018). Seedlings were grown and oxygen uptake measured at the indicated temperature. For all genotypes and at both temperatures, the shape of the profile of uptake along the root was similar (Figure 3). Likewise, for all genotypes and nearly all positions, oxygen uptake rates at 25°C were higher than those at 15°C, showing that oxygen uptake was in general far from being homeostatic. Oxygen uptake was maximal at the origin, taken as the quiescent center of the root, a location where most of the cells in the cross-section are part of the root cap (Dolan et al., 1993). With increasing distance from the quiescent center, uptake rate fell, becoming roughly constant by around 800 μm from the tip. The maximum oxygen uptake rate at the position of the quiescent center implies this region has a greater demand for energy than have the adjacent meristem cells.

3.3 | Effect of root geometry on vibrating probe measurements

The canonical equation for converting vibrating-probe measurements to flux, Equation (1) (Newman, 2001), assumes a cylindrical root of infinite length; but, a root is finite and tapering at the end. We examined whether the deviation from the assumed geometry could account for elevated uptake rates where the root tip tapers, reported by us (Figure 3) and by others (e.g., McLamore et al., 2010; Mugnai et al., 2012). To do so theoretically, we constrained oxygen uptake to occur at a constant rate per unit volume of root, and applied that to a model root, matching the geometry of the real root (see Section 2).

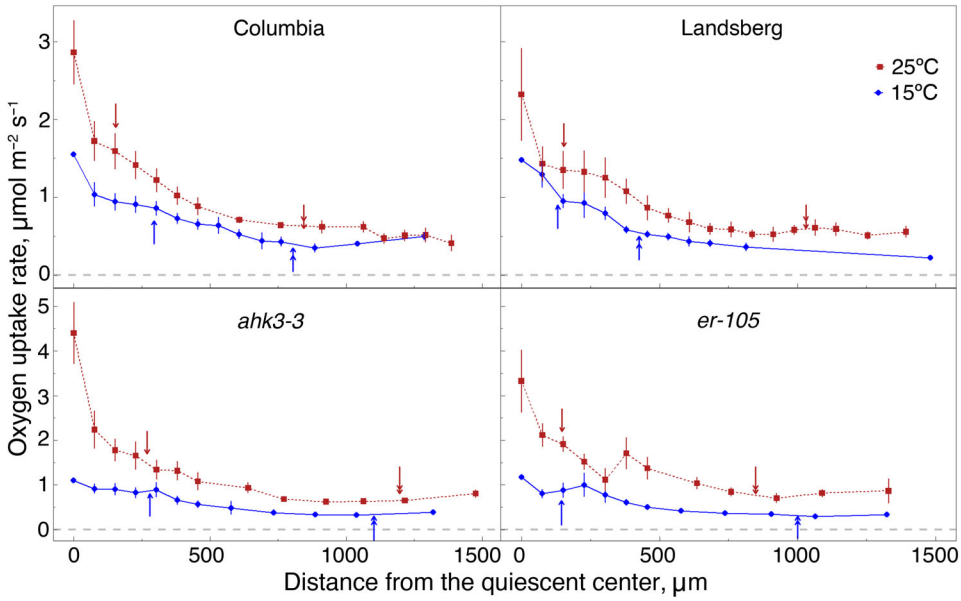

FIGURE 3 Oxygen uptake rate as a function of position for plants grown and measured at either 25°C (red symbols) or 15°C (blue symbols). Oxygen uptake rate, determined from vibrating probe output (i.e., the measured flux, *J*; see Section 2), is represented as moles of oxygen taken up per unit cross-sectional area of root and time. Symbols plot mean ± SE of 9–11 roots. Single arrows mark the boundary between meristem and elongation zone and double arrows mark the shootward side of the elongation zone, taken as the average for the treatment (see Figure 6). A mixed ANOVA with a linear mixed-effects model was used to determine if there were significant differences between the different genotypes at each temperature and location. At 15°C there were no significant differences in oxygen uptake between genotypes at any location measured along the root. At 25°C there were significant differences in oxygen uptake between all genotypes only at the quiescent center (p <0.05), except between Columbia and Landsberg

With the ratio of measured to modeled uptake in the shootward cylindrical region taken as unity, the measured rate is higher than the modeled rate, by as much as six-fold at the tip (Figure 4A). Thus, failure to account for the finite, tapering shape of the root tip actually underestimates the real rate, by as much as a factor of two.

To examine the effect of geometry experimentally, we built an artificial root by using an agarose substrate impregnated uniformly with yeast. The agarose substrate had a cylindrical region adjoined to a tapering region (Figure 4B). The vibrating probe was translated across both regions, keeping the distance from the probe to the agarose surface constant, as was done for real roots. Consistent with the model, as the probe moved over the tapering region, oxygen uptake rate decreased, along with the lowered volume of respiring material (Figure 4C). Thus, the angled and finite geometry again appears unlikely to artifactually elevate the measured rate of uptake. Taken together, theory and experiment both support the conclusion that the measured maximal rate of oxygen uptake around the quiescent center is real.

3.4 | Defining root growth zones

To be able to relate the measured rates of oxygen uptake to cell division and elongation, we obtained the distribution of growth in the same experiments in which oxygen uptake was measured and on the same roots. To do so, we imaged the root at various times during oxygen uptake measurements, and used these images to obtain a velocity profile for each root (Figure 5). As shown, the velocity profile is plotted with transformed coordinates: in this root-centric frame, the quiescent center is motionless ($x = 0$, $v = 0$) and the maturation zone moves away at a constant rate that equals the rate of root growth (Baskin & Zelinsky, 2019; Silk, 1992). In the example shown, velocity plateaued around 1 mm from the tip, a position that indicates the transition from elongation to maturation zone. Closer to the tip, there is another transition, in this case around 0.15 mm from the quiescent center. This transition divides the growth zone into two regions: a rootward region where velocity increases gradually with position and a shootward region where velocity increases steeply. The latter corresponds to the elongation zone and the former to the meristem (plus adjacent transition zone). The x-axis values for the two transition points were obtained by curve fitting (see Section 2).

For Columbia, consistent with a previous report (Yang et al., 2017), the meristem was shorter at the higher temperature and the length of the elongation zone was roughly the same at both temperatures (Figure 6). By contrast, for Landsberg, the size of the meristem was roughly the same at both temperatures, while the elongation zone was longer at 25°C than at 15°C, showing that in this background neither cell production rate (Figure 2) nor growth zone length (sum of meristem and elongation zone lengths; Figure 6) acclimated to these temperatures. Interestingly, while both *ahk3-3* and *er-105* had nearly doubled cell production rates when compared with the wild type (Columbia) (Figure 2), both had similar elongation zone and meristem lengths at the two temperatures (Figure 6). Since Landsberg, *ahk3-3*, and *er-105* all lack temperature-acclimated cell

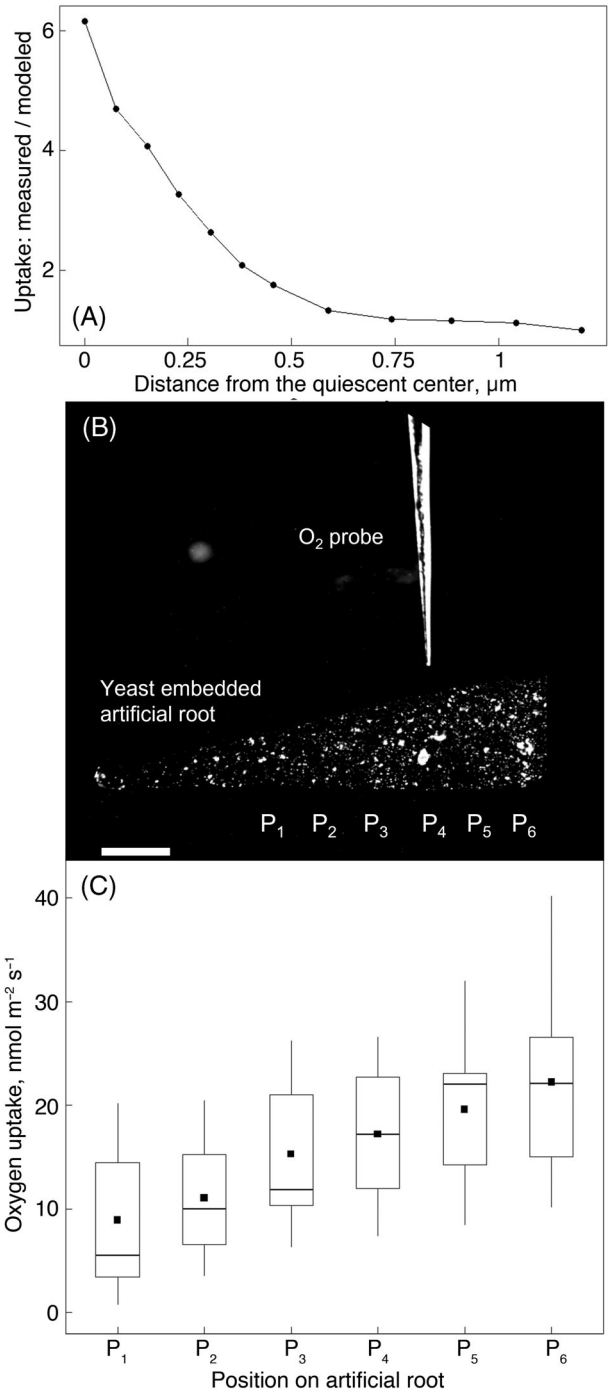

FIGURE 4 Effect of root geometry on measured oxygen uptake rate. (A) Theoretical. Oxygen uptake was modeled assuming equal uptake per unit volume of root and a geometry fitted to that of a real root (see Section 2). Uptake at each position is plotted as the ratio of that measured for Columbia at 25°C divided by the modeled rate. (B,C) Experimental. (B) Dark-field micrograph of an artificial root in relation to the vibrating probe. P_1–P_6 show approximate positions where uptake was measured, with P_1–P_3 in the tapering region and P_4–P_6 in the cylindrical region. Scale bar = 780 µm. (C) Measured oxygen uptake (measured as for Figure 3). The square symbol shows the mean, while the box and whiskers show the data distribution, and the horizontal black lines are the median for measurements on six artificial roots. The average radius at P_1–P_6 was: 156, 234, 312, 390, 390, and 390 µm, respectively

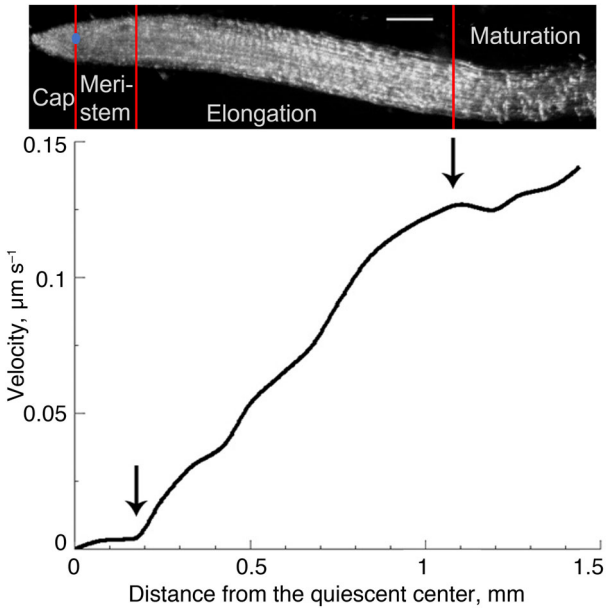

FIGURE 5 Growth analysis. (Top) Representative image of a root (*er-105* at 15°C) shown at roughly the same scale as represented by the x-axis in the plot below, with the approximate boundaries of each zone delineated by red lines. The position of the quiescent center is indicated approximately by a blue square. Bar = 100 µm. (Bottom) Velocity profile for the exemplary root immediately prior to oxygen uptake measurements. The profile is subsequently fitted to a function that defines the two transitions indicated by arrows (described in Section 2)

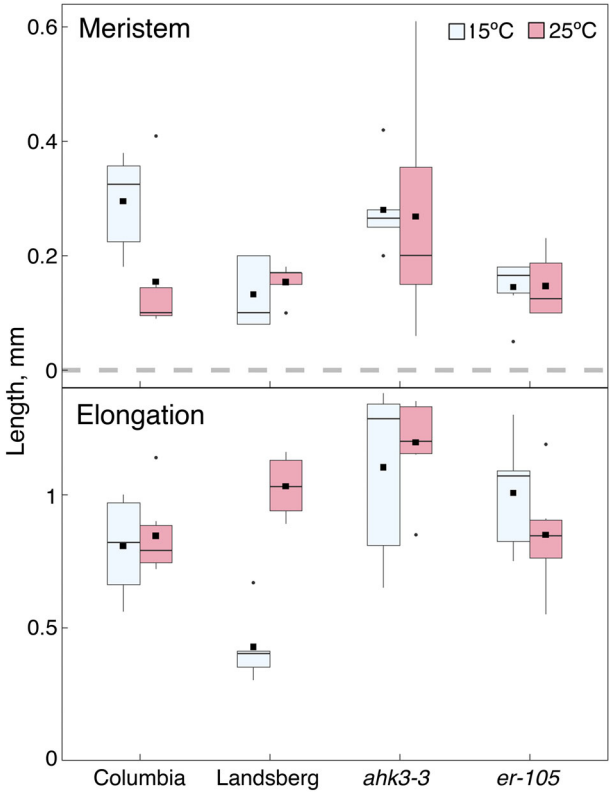

FIGURE 6 Zone lengths obtained from the velocity profiles for the roots used for oxygen uptake measurements. Data plotted as for Figure 2. Sample sizes were 5–7 roots

production rates, but have similar meristem length at the two temperatures, this could imply that meristem length is being acclimated rather than cell production rate. With the caveat that sample sizes are small and variable, these results suggest that in response to temperature, processes that acclimate growth zone length do so independently of those acclimating cell production rate and that acclimation of growth zone length requires neither AHK3 nor erecta kinase.

3.5 | Oxygen uptake rate in functionally defined zones

With meristem and elongation zone thus delineated, we evaluated oxygen uptake rate for each zone by numerically integrating the profile of oxygen uptake rate of each root from one end of the zone to the other. The quiescent center was evaluated at the first point of the profile only. In addition, we summed integrated oxygen uptake rate for all three zones (Figure 7). For a few roots where reliable velocity profiles could not be obtained, the transition points defining the zones were taken as the average for the given genotype and temperature. Then, to readily compare the responses, we calculated ratios for the two temperatures for each of the treatments in Figure 7 (Table 1). This ratio compares steady-state rates at two temperatures, rather than rates following a shift in temperature, and was named LTR_{10} by Larigauderie and Körner (1995). Because this acronym is not well known, we will call the ratio a *steady-state* Q_{10}.

Over the whole growth zone (i.e., the sum), integrated oxygen uptake at 25°C was greater than at 15°C for all genotypes (Figure 7), with steady-state Q_{10} values ranging from 1.8 (Columbia) to 3 (Landsberg) (Table 1). These data suggest that respiration in the growing regions of these roots generally does not acclimate to temperature, at least as shown by measurement at the growing temperature. The steady-state Q_{10} values for both Landsberg and *er-105* were significantly greater than that of Columbia. Thus, the growing regions of Landsberg roots appear to be more thermally sensitive than those of Columbia, an effect that can be attributed at least in part to loss of the erecta kinase.

In the quiescent center, which at a single position took up oxygen to about the same extent as did the entire meristem (Figure 7), the steady-state Q_{10} values were around 2, except for that of *ahk3*, which was 4 (Table 1), revealing an unexpected respiratory phenotype for plants harboring this mutation.

As for the meristem, integrated oxygen uptake was lower than that of the elongation zone and generally less affected by temperature (Figure 7). In the Columbia meristem, oxygen uptake was actually *lower* at 25 than 15°C, a decrease that parallels the shortened length of the meristem (Figure 6). Among the four genotypes, steady-state Q_{10} values for the meristem ranged from 0.7 to 2.1 (Table 1). These values trended smaller than those of the elongation zone, significantly so for Columbia and *er-105*.

When considered over its entirety, the elongation zone can be seen to account for the majority of oxygen consumption by the growing regions of the root, particularly at 25°C (Figure 7). While this at least partially reflects the fact that the elongation zone is longer than the other zones, oxygen uptake of the elongation zone dominated the total even for Landsberg at 15°C, where meristem and elongation zone had roughly similar lengths (Figure 6). Appreciable respiratory demand for the elongation zone can also be seen from the steady-state Q_{10}, which ranged from 2.6 to 3.3. (Table 1; none of the genotypes differed significantly from Columbia).

3.6 | Mitochondrial density as a function of position

We were surprised by the quiescent center taking up oxygen so much faster than any other measured position (Figure 3), implying that cells in this region respire faster than those in the adjacent meristem. We reasoned that a greater respiration predicts a greater density of mitochondria. To examine mitochondrial density, we observed fluorescence from a Columbia line in which YFP is localized to that organelle by fusion to a signal sequence (Nelson et al., 2007). Consistent with the oxygen uptake profile, fluorescent intensity was maximal at the root cap and declined markedly with distance toward the shoot (Figure 8A).

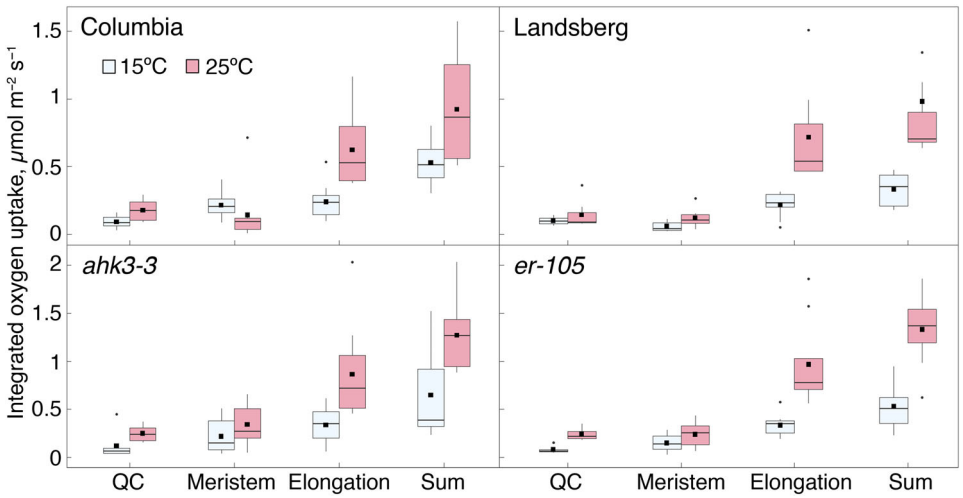

FIGURE 7 Integrated oxygen uptake within functional zones. Uptake profiles were interpolated linearly between each uptake data point and integrated numerically. Data for the quiescent center ("QC") was taken as a single strip. Data plotted as for Figure 2. One upper outlier at was removed from the plot for the Landsberg sum, although accounted for in the average. Sample size is 9–11 roots, per genotype

TABLE 1 Steady-state Q_{10} values for integrated oxygen uptake as a function of genotype and root zone

Genotype	Quiescent center	Meristem	Elongation zone	Sum
Columbia	1.8 ± 0.4^{y}	0.7 ± 0.3^{x}	2.6 ± 0.5^{y}	1.8 ± 0.3^{y}
Landsberg	1.6 ± 0.5^{x}	$2.1 \pm 0.6^{*}$	3.3 ± 0.8^{y}	$3.0 \pm 0.6^{y,*}$
ahk3-3	$4.0 \pm 0.9^{x,*}$	$1.6 \pm 0.6^{y,*}$	2.6 ± 0.7	2.0 ± 0.5^{y}
er-105	2.8 ± 0.7	$1.6 \pm 0.5^{x,*}$	2.9 ± 0.6^{y}	$2.5 \pm 0.5^{*}$

Note: The values were calculated as the average integrated oxygen uptake rate (Figure 7, black squares) for roots grown and measured at 25°C divided by that for roots grown and measured 15°C. The errors are ±1 SE, which was calculated based on the standard formula for error propagation (Gardenier et al., 2011). For comparison among zones for a given genotype, different letters (x, y) indicate equivalence of means is rejected with $p < 0.05$ by a two-tailed t test. For comparison among genotypes for a given zone, the "*" denotes that equivalence to the Columbia mean is rejected with $p < 0.05$ by a two-tailed t test.

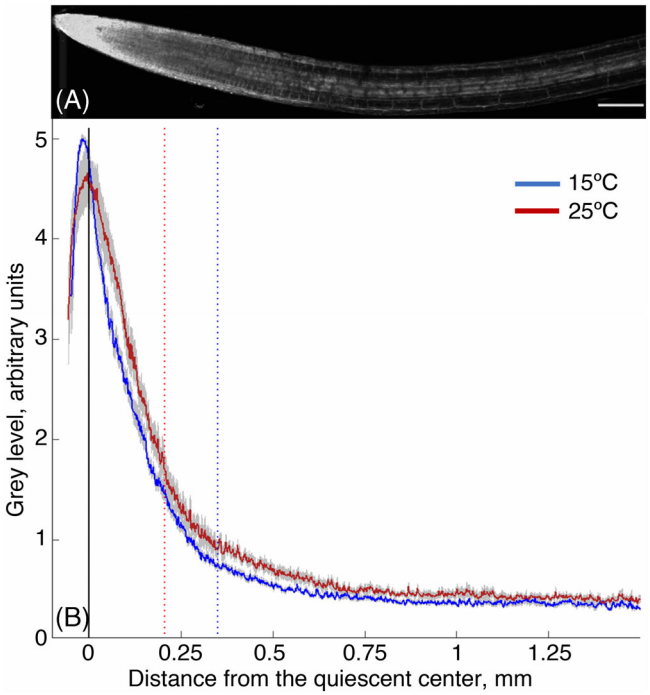

FIGURE 8 Mitochondrial fluorescence as a function of position. (A) Representative fluorescence micrograph of the root of a seedling expressing a mitochondrially localized YFP and grown at 25°C. Bar = 100 μm. (B) Mean gray level (i.e., fluorescence intensity; solid lines) ± SE (gray shading) for 10 roots at each temperature. Dotted vertical lines signify the shootward boundary of the meristem as reported by Yang et al. (2017) for 15°C (blue) and 25°C (red). Data from Yang et al. are used because they apply to seedlings grown at UMass, as for this figure. The image in A is positioned to coincide approximately with the x-axis in B. Measured gray levels were divided by 10,000

Quantifying fluorescence intensity confirms visual impression (Figure 8B). Maximal fluorescence occurred on the root-cap side of the quiescent center and fell precipitously through the meristem. The pattern of fluorescence was generally similar at the two temperatures. If anything, the intensity decreased in 15°C-grown roots a little more rootward of the decrease in those grown at 25°C (Figure 8), opposite of the change in meristem size (Figure 6; Yang et al., 2017). That mitochondrial density plummets along the meristem is consistent with the conclusion above that cell division places only modest demands on the energy budget. The decrease in intensity between 0 and ~200 μm cannot be explained by dilution due to vacuole formation because in this region vacuole volume is small and relatively constant. Evidently, the root cap is enriched in mitochondria, suggesting that this tissue is a major consumer of energy within the root.

4 | DISCUSSION

While our understanding of how temperature influences respiration in developing leaves is growing (Dusenge et al., 2018; Tcherkez et al., 2012), less is known about how temperature impacts rates of respiration within growing regions of roots. This gap in understanding has consequences for our ability to model the carbon cycle. Roots grow actively and within and near the growth zone exude appreciable quantities of carbon into the rhizosphere (Vives-Peris et al., 2020); hence, in missing root development, models of how respiration rate in plants responds to moderate temperature change are incomplete. This incomplete understanding matters, as roots contribute 30%–50% of the carbon dioxide released by whole plant respiration (Poorter et al., 1990) and up to 60% of total soil efflux (Hanson et al., 2000). Globally, plant respiration releases approximately 60 gigatons of carbon into the atmosphere each year (Field, 2001; Schlesinger, 1997)—5 to 10 times more than released by anthropogenic processes. Thus, to model the impacts of global climate warming on the carbon cycle, we need a more complete understanding of how respiration in roots varies in response to growth temperature. By highlighting the impacts of growth temperature on respiration of the growing regions of roots, our study makes an important contribution to helping illuminate the 'hidden half' of plant respiration.

4.1 | Oxygen vibrating probe measurements and respiration

By measuring elongation and oxygen uptake in the same roots at the same time, we aimed to compare growth parameters and respiration. We take the rate of oxygen uptake measured by the vibrating probe to reflect respiration rate and hence energy supply. We recognize that doing so is a simplification. Some oxygen might be supplied from the shoot, in which case our measured uptake rates will underestimate local

consumption; we note that air spaces are infrequent if not absent in *A. thaliana* seedling roots (Dyson et al., 2014). To the extent that the measured regions differ in permeability, the relation between measured oxygen uptake and underlying respiration will differ. Although the measured regions mainly have thin and permeable primary cell walls, they might differ in the abundance of membrane channels that permeate oxygen, such as aquaporins (Zwiazek et al., 2017), and the root cap might be sheathed in mucilage. Furthermore, oxygen is also consumed by reactions that do not make ATP (such as catalyzed by the mitochondrial alternative oxidase) or might diffuse out into the stele and hence transpiration stream; the magnitude of such losses presumably would differ among regions of the root. Nevertheless, we consider ascribing oxygen uptake to respiration to be a reasonable first approximation.

Converting a flux measured by the vibrating probe to a respiration rate requires that the oxygen gradient be stable. Instability can be caused by physical factors, such as fluid flow within the boundary layer or unidirectional diffusion from the air-water surface. We do not think these factors apply here because the root was 14 mm from the surface, too far for diffusion over the hour of measurement, and was, except for its own growth, motionless.

Instability can also be caused by biological factors, for example metabolic changes in response to submergence. We believe that the gradient was stable over the hour needed for measurement here for several reasons. First, as described in Section 2.3, typical signs of instability among raw probe data were absent. Second, although submergence conjures up images of suffocation, roots growing in soil experience oxygen concentrations notably lower than those of air because of microbial respiration and chemical reactions that bind oxygen. Third, oxygen consumption measured here is higher than that commonly measured for root systems in soil. A flux measurement of 1 μmol m^{-2} s^{-1}, which typifies the elongation and mature zones (Figure 3), converted to volumetric units (by multiplying by 2/radius) of dry mass (by assuming a fresh mass density of 1 g cm^{-3} and that dry mass equals 10 % of fresh mass) becomes 400 nmol g^{-1} s^{-1}. This value is substantially higher than typically reported for whole root systems in soil at 25°C (e.g., Loveys et al., 2003, report rates around 40 nmol g^{-1} s^{-1} for roots of 9 species). Given that the magnitude of the apparent respiration rate measured here is comparatively high, we consider that the roots in our setup are likely to be receiving a customary supply of oxygen.

4.2 | Oxygen uptake at the root cap

We report that oxygen uptake rate per cross-sectional area was greatest at the origin (Figure 3). For our experiments, the origin was sited at the quiescent center of the root. In *A. thaliana*, the quiescent center comprises four cells, encircled by a ring of initial cells, which are in turn encircled by layers of lateral root cap cells (Dolan et al., 1993). As the origin, we chose the quiescent center rather than the tip of the root cap because the position of the center is easily seen through the microscope and because the length of the root cap varies as tiers of root cap cells are periodically shed. The quiescent center constitutes a reliable origin for measurements but most of the cells at this position belong to the root cap.

Consistently, in vibrating probe studies of maize, bamboo, soybean, and broad bean, maximal oxygen uptake was reported to occur between 0.2 and 0.5 mm from the apex (McLamore et al., 2010, 2017), which in these species is expected to be in the root cap. By contrast, in another report on maize, oxygen uptake was maximal at the approximate position of the meristem, with a small peak in the presumptive root cap (Mugnai et al., 2012). The reason for the discrepancy between the two reports on maize is not understood. Consistent with maximal uptake at the root cap in maize, oxygen concentration in the root cap is essentially zero even while neighboring regions are partly or fully oxygenated (Armstrong et al., 1994). We conclude that, in general, the root cap consumes oxygen at the highest rate among root tissues.

We argue that the high oxygen uptake rate seen here at the origin, and by others in the presumptive root cap, reflects an underlying high metabolic activity of this tissue. First, we show that the high rate is unlikely to be an artifact of assuming infinite, cylindrical geometry, and in fact might be an underestimate (Figure 4). Second, root cap cells are busy, responding to signals and copiously secreting organic compounds into the rhizosphere (Vives-Peres et al., 2020). Third, the cap had the highest density of mitochondria (Figure 8). Consistently, in maize roots, root cap cells have a greater density of mitochondria than those of the in the quiescent center, based on electron microscopy (Clowes & Juniper, 1964), and mitochondria specifically in the quiescent center have reduced activity (Jiang et al., 2006). Fourth, quiescent center cells were so named because of their limited metabolic activity, which plausibly extends, in *A. thaliana*, to the surrounding initial cells. Stem cells of all kinds are thought to limit metabolism to minimize genetic damage that might arise from reactive oxygen or other byproducts (Rumman et al., 2015). Recently, the importance of hypoxia for signaling stem cell identity has been emphasized for plant meristems (Weits et al., 2021). If so, quiescent center cells are likely to consume oxygen sparingly and, in turn, would benefit from a voracious consumption by surrounding root cap cells.

4.3 | Thermal sensitivity of the two mutants

Both *er-105* and *ahk3-3* were more sensitive to growth temperature than were their genetic background (Columbia). For *er-105*, this is evident from the steady-state Q_{10} for oxygen uptake summed over the growth zone being significantly greater than that of Columbia (Table 1). This trait was similar in Landsberg, which also carries a mutated copy of the erecta kinase, and resulted mainly from stimulated respiration in the elongation zone. Finding heightened thermal sensitivity in *erecta* roots might be consistent with roles attributed to the kinase in mediating responses to temperature of the shoot (Patel et al., 2013; Qi et al., 2004; Shen et al., 2015).

For *ahk3-3*, the heightened thermal sensitivity is seen from the oxygen uptake at the quiescent center, which had a steady-state Q_{10} of 4 (Table 1). Outside of this region, the steady-state Q_{10} in *ahk3-3*

resembled that of the wild type and indeed the line produced cells reliably and grew if anything faster than did Columbia (Figure 2; also reported previously: Pernisova et al., 2016) implying that the line is vigorous. AHK3 is a membrane receptor that responds to the hormone, cytokinin; but, because the plant has several such receptors, phenotypes of single mutants are generally weak to nonexistent (Bartrina et al., 2017). Although the root cap contains plenty of cytokinin (Aloni et al., 2004; Antoniadi et al., 2015), to our knowledge, the only regulatory activity ascribed to this hormone specifically within the root cap is gravitropism (Aloni et al., 2006; Schaller et al., 2015). In our hands as well as in others' (Pernisova et al., 2016), *ahk3* roots have a wild-type gravitropism. Therefore, cytokinin appears to influence root cap metabolism via activities that are currently unknown.

4.4 | Relationship between oxygen uptake and elongation

To our knowledge, the spatial distribution of oxygen uptake and elemental elongation rate have been measured concomitantly only once before (Mancuso & Boselli, 2001). In adventitious roots of three species of *Vitis* (grape), those authors reported that oxygen uptake varies bimodally, with a first and smaller peak at ~0.75 mm from the tip, a valley reaching almost zero uptake at ~1.25 mm from the tip, and then a large and broad peak, centered at 2.5 mm from the tip. The first peak is likely to be at or near the quiescent center, which thus resembles the results here. However, the broad elevation of oxygen uptake rate centered on the elongation zone differs from the continuously declining profiles reported here (Figure 3). The reason for the discrepancy between our data and those of Mancuso and Boselli is not clear but might reflect the different species, root type (primary vs. adventitious roots), or vibrating probe methodology. Nevertheless, albeit without accompanying growth data, profiles of oxygen uptake for onion, maize, soybean, broad bean, and bamboo all show oxygen uptake as being roughly constant across the putative elongation zone and lower than at the tip (McLamore et al., 2010, 2017; Mugnai et al., 2012; Norris Jr. et al., 1959). Evidently, the oxygen uptake peak in the elongation zone of grape roots observed by Mancuso and Boselli (2001) is unusual.

Across the elongation zone, although oxygen uptake per cross-sectional area declined to a plateau (Figure 3), uptake per cell undoubtedly increased. Increased demand per cell is indicated by realizing that the average oxygen uptake fell by about two-fold from one end of the zone of elongation to the other (i.e., ~200 to ~1200 μm from the quiescent center; Figure 3) but at the same time cell length increased five- to ten-fold (Yang et al., 2017). Insofar as the massive increase in volume is water, the measured oxygen uptake declining over the elongation zone by only two-fold implies that, as reported previously for root segments (Norris Jr. et al., 1959), respiration rate per gram of cytoplasmic protein increased substantially. Consistently, integrated oxygen uptake in the elongation zone is higher than in the meristem, despite the elongation zone containing far fewer cells (Yang et al., 2017). Finally, the fluorescence intensity from mitochondria was roughly constant across the elongation zone, a constancy that predicts synthesis of mitochondria to balance their dilution and displacement away from the tip caused by elongation (Silk, 1992).

Even though cells in the elongation zone consumed more oxygen than did their meristematic neighbors, the energy might be needed for more than the process of rapid elongation. Compared to a densely cytoplasmic cell, a cell with a giant central vacuole might have higher maintenance costs, through transporting material both into and throughout the cell (Lambers et al., 2008). Several lines of evidence imply that rapid elongation itself is not expensive. First, some synthetic work to support rapid elongation seems to be accomplished in the meristem, for example synthesizing osmolytes and precursors of cell wall polymers (Wu et al., 1994). Second, here, over the hour of measurement, elongation rate decreased, presumably because of a gravitropic response to the root's horizontal placement; however, oxygen uptake showed no similar decline. Finally, here (Figure 3) and other reports where oxygen uptake has been measured as a function of position in the root (McLamore et al., 2010; Mugnai et al., 2012; Norris Jr. et al., 1959), the profiles of uptake rate rarely if ever decrease in the region where cells presumably cease elongating, implying that the high respiratory rate per cell is sustained into the maturation zone and thus not tied directly to the elongation process itself.

4.5 | Relationship between oxygen uptake and cell division

Oxygen uptake by the meristem correlated poorly with cell division. While meristem size was considerably shorter at the warmer temperature for Columbia, the profiles of oxygen uptake versus position were congruent at the two temperatures, giving no hint of the difference in meristem length (Figure 3). Similarly, meristem length was unrelated to the profile of mitochondrial abundance (Figure 8). In Columbia, cell production rate was the same at both growth temperatures (Figure 2) but oxygen uptake in the meristem was lower at 25°C (Figure 7), inconsistent with division being costly. Similarly, at 15°C, Columbia and Landsberg meristems produced cells at similar rates, but the Columbia meristem took up more oxygen. Finally, in the two mutants, cell production rate at 25°C was stimulated to a greater extent than for Landsberg (Figure 2) but the steady-state Q_{10} values for oxygen uptake in the meristem were not different among these three lines (Table 1). Taken together, these data suggest that the respiratory demands of cell division are modest.

A modest energy demand for cell division might be surprising, given the doubling of cell content and the notable cost of protein synthesis (e.g., Amthor et al., 2019). One explanation might be that meristem cells expend less energy on transport across membranes than do cells in neighboring zones. To our knowledge, the costs of specific metabolic activities of root meristem cells have been little explored, particularly for intact preparations. Hypoxia decreases division in roots (Amoore, 1962; López-Sáez et al., 1969), but the decrease might reflect a global response to hypoxia rather than a direct effect of lowered

respiration. Here, steady-state Q_{10} values for the meristem tended to be lower than those for the elongation zone or the quiescent center (Table 1). Conceivably, the lower Q_{10} indicates the existence of acclimation machinery that allows demands from cell division to be met more efficiently. In that light, the shortened meristem in Columbia at 25°C and hence the limited cell production rate, might be considered as an alternative or additional adaptation to save energy. But, a cell leaving the meristem enters the elongation zone, where energetic demands are apparently larger, a transfer that would seem to limit the usefulness of meristem truncation for energy conservation.

5 | CONCLUSIONS

We undertook this study to determine whether the constancy with growth temperature of cell production rate and growth zone length, observed for the roots of *A. thaliana* (Columbia), could be accounted for by energetics. We find little evidence that cell division is costly, implying that energetics do not underlie the acclimatizing cell production. As for elongation, we find that the steady-state Q_{10} for oxygen uptake in the elongation zone tends to be around three, implying a higher than average cost for this zone and little evidence for thermal acclimation. Here, energetics might account for the constancy of growth zone length. However, rather than the process of elongation, the cost might be incurred by the requirements of supporting a large cell size, and if so, then the boundary between elongation and mature zones would have little energetic consequence. Our conclusions could be profitably extended by developing systems where cell division and elongation can be manipulated directly while oxygen uptake rates are measured.

ACKNOWLEDGMENTS

This work was supported by the Australian Research Council Centre of Excellence in Plant Energy Biology, an Australian Research Council Grant (CE140100008) to Stephen D. Tyerman, the UMass Interdepartmental Graduate Program (IDGP) travel fund, the IDGP Graduate Opportunity Fellowship, the Albert L. Delisle Scholarship, and the Gilgut Fellowship. During manuscript preparation, Maura J. Zimmermann was supported by the US National Science Foundation grant IOS—2035814 to Tobias I. Baskin. We thank Dr. Wendy Sullivan, University of Adelaide, for her technical assistance, and Dr. Andreas Nebenführ, University of Tennessee, for providing us with the marker line for mitochondria.

AUTHOR CONTRIBUTIONS

Tobias I. Baskin conceptualized the project, along with Owen K. Atkin and Stephen Tyerman. Maura Zimmermann performed the experiments, analyzed the data, and drafted the manuscript. Jayakumar Bose aided with experiments and developed the artificial root. Eric M. Kramer modeled the effect of geometry. All authors helped revise the manuscript draft. All authors have read and approved the manuscript.

DATA AVAILABILITY STATEMENT

The data that support the findings of this study are available from the corresponding author upon reasonable request.

ORCID

Tobias I. Baskin https://orcid.org/0000-0001-5189-3310

REFERENCES

Aloni, R., Langhans, M., Aloni, E. & Ullrich, C.I. (2004) Role of cytokinin in the regulation of root gravitropism. *Planta*, 220, 177–182.

Amoore, J.E. (1962) Oxygen tension and the rates of mitosis and interphase in roots. *Journal of Cell Biology*, 13, 365–371.

Amthor, J.E. (1984) The role of maintenance respiration in plant growth. *Plant Cell & Environment*, 7, 561–569.

Amthor, J.S., Hanson, A.D., Millar, A.H., Stitt, M., Sweetlove, L.J. & Tyerman, S.D. (2019) Engineering strategies to boost crop productivity by cutting respiratory carbon loss. *Plant Cell*, 31, 297–314.

Andrews, M. (1997) Equilibrium charge density on a conducting needle. *American Journal of Physics*, 65, 846–950.

Antoniadi, I., Plačková, L., Simonovik, B., Doležal, K., Turnbull, C., Ljung, K. et al. (2015) Cell-type specific cytokinin distribution within the arabidopsis primary root apex. *Plant Cell*, 27, 1955–1967.

Armstrong, A.F., Logan, D.C. & Atkin, O.K. (2006) On the developmental dependence of leaf respiration: responses to short- and long-term changes in growth temperature. *American Journal of Botany*, 93, 1633–1639.

Armstrong, W., Strange, M.E., Cringle, S. & Beckett, p.M. (1994) Microelectrode and modelling study of oxygen distribution in roots. *Annals of Botany*, 74, 287–299.

Atkin, O.K., Bruhn, D., Hurry, V.M. & Tjoelker, M.G. (2005) The hot and the cold: unravelling the variable response of plant respiration to temperature. *Functional Plant Biology*, 32, 87–105.

Atkin, O.K., Edwards, E.J. & Loveys, B.R. (2000) Response of root respiration to changes in temperature and its relevance to global warming. *New Phytologist*, 147, 141–154.

Bartrina, I., Jensen, H., Novák, O., Strnad, M., Werner, T. & Schmülling, T. (2017) Gain-of-function mutants of the cytokinin receptors AHK2 and AHK3 regulate plant organ size, flowering time and plant longevity. *Plant Physiology*, 173, 1783–1797.

Baskin, T.I. (2013) Patterns of root growth acclimation: constant processes, changing boundaries. *WIREs Developmental Biology*, 2, 65–73.

Baskin, T.I. & Wilson, J.E. (1997) Inhibitors of protein kinases and phosphatases alter root morphology and disorganize cortical microtubules. *Plant Physiology*, 113, 493–502.

Baskin, T.I. & Zelinsky, E. (2019) Kinematic characterization of root growth by means of stripflow. In: Cvrčková, F. & Žárský, V. (Eds.) *Plant cell morphogenesis: methods and protocols*, 2nd edition. New York, NY: Humana Press, pp. 291–305.

Bidel, L.p.R., Renault, P., Pagès, L. & Rivière, L.M. (2001) An improved method to measure spatial variation in root respiration: application to the taproot of a young peach tree, *Prunus persica*. *Agronomie*, 21, 179–192.

Bingham, I.J., Panico, A. & Stevenson, E.A. (1996) Extension rate and respiratory activity in the growth zone of wheat roots: time-course for adjustments after defoliation. *Physiologia Plantarum*, 98, 201–209.

Borrill, P. (2020) Blurring the boundaries between cereal crops and model plants. *New Phytologist*, 228, 1721–1727.

Bouma, T.J., Nielsen, K.L., Eissenstat, D.M. & Lynch, J.P. (1997) Estimating respiration of roots in soil: interactions with soil CO_2, soil temperature and soil water content. *Plant and Soil*, 195, 221–232.

Clowes, F.A.L. & Juniper, B.E. (1964) The fine structure of the quiescent centre and neighbouring tissues in root meristems. *Journal of Experimental Botany*, 15, 622–630.

Darwent, M.J., Armstrong, W., Armstrong, J. & Beckett, p.M. (2003) Exploring the radial and longitudinal aeration of primary maize roots by means of Clark-type oxygen microelectrodes. *Russian Journal of Plant Physiology*, 50, 722–732.

Dolan, L., Janmaat, K., Willemsen, V., Linstead, P., Poethig, S., Roberts, K. et al. (1993) Cellular organisation of the *Arabidopsis thaliana* root. *Development*, 119, 71–84.

Dusenge, M.E., Duarte, A.G. & Way, D.A. (2018) Plant carbon metabolism and climate change: elevated CO_2 and temperature impacts on photosynthesis, photorespiration and respiration. *New Phytologist*, 22, 32–49.

Dyson, R.J., Vizcay-Barrena, G., Band, L.R., Fernandes, A.N., French, A.P., Fozard, J.A. et al. (2014) Mechanical modelling quantifies the functional importance of outer tissue layers during root elongation and bending. *New Phytologist*, 202, 1212–1222.

Field, C.B. (2001) Plant physiology of the 'missing' carbon sink. *Plant Physiology*, 125, 25–28.

Fricke, W. (2017) Water transport and energy. *Plant, Cell and Environment*, 40, 977–994.

Gardenier, G.H., Gui, F. & Demas, J.N. (2011) Error propagation made easy—or at least easier. *Journal of Chemical Education*, 88, 916–920.

Grif, V.G., Ivanov, V.B. & Machs, E.M. (2002) Cell cycle and its parameters in flowering plants. *Tsitologia*, 44, 936–980.

Hanson, p.J., Edwards, N.T., Garten, C.T. & Andrews, J.A. (2000) Separating root and soil microbial contributions to soil respiration: a review of methods and observation. *Biogeochemistry*, 48, 115–146.

Henriksen, G.H., Raman, D.R., Walker, L.P. & Spanswick, R.M. (1992) Measurement of net fluxes of ammonium and nitrate at the surface of barley roots using ion-selective microelectrodes. II. Patterns of uptake along the root axis and evaluation of the microelectrode flux estimation technique. *Plant Physiology*, 99, 734–747.

Huang, B., Rachmilevitch, S. & Xu, J. (2012) Root carbon and protein metabolism associated with heat tolerance. *Journal of Experimental Botany*, 63, 3455–3465.

Jensen, W.A. & Ashton, M. (1960) Composition of developing primary wall in onion root tip cells. I. Quantitative analyses. *Plant Physiology*, 35, 313–323.

Jiang, K., Ballinger, T., Li, D., Zhang, S. & Feldman, L. (2006) A role for mitochondria in the establishment and maintenance of the maize root quiescent center. *Plant Physiology*, 140, 1118–1125.

Lambers, H., Chapin, F.S. & Pons, T.L. (2008) *Plant physiological ecology*. New York, NY: Springer.

Larigauderie, A. & Körner, C. (1995) Acclimation of leaf dark respiration to temperature in alpine and lowland plant species. *Annals of Botany*, 76, 245–252.

López-Sáez, J.F., González-Bernáldez, F., González-Fernández, A. & García-Ferrero, G. (1969) Effect of temperature and oxygen tension on root growth, cell cycle and cell elongation. *Protoplasma*, 67, 213–221.

Loveys, B.R., Atkinson, L.J., Sherlock, D.J., Roberts, R.L., Fitter, A.H. & Atkin, O.K. (2003) Thermal activation of leaf and root respiration: an investigation comparing inherently fast- and slow-growing species. *Global Change Biology*, 9, 895–910.

Loveys, B.R., Scheurwater, I., Pons, T.L., Fitter, A.H. & Atkin, O.K. (2002) Growth temperature influences the underlying components of relative growth rate: an investigation using inherently fast- and slow-growing plant species. *Plant Cell & Environment*, 25, 975–987.

Luxmoore, R.J., Stolzy, L.H. & Letey, J. (1970) Oxygen diffusion in the soil-plant system. II. Respiration rate, permeability, and porosity of consecutive excised segments of maize and rice roots. *Agronomy Journal*, 62, 322–324.

Mancuso, S. & Boselli, M. (2001) Characterization of the oxygen fluxes in the division, elongation and mature zones of *Vitis* roots: influence of oxygen availability. *Planta*, 214, 767–774.

McLamore, E.S., Jaroch, D., Chatni, M.R. & Porterfield, D.M. (2010) Self-referencing optrodes for measuring spatially resolved, real-time metabolic oxygen flux in plant systems. *Planta*, 232, 1087–1099.

McLamore, E.S., Porterfield, D.M. & Wan, Y. (2017) Measuring spatial and temporal oxygen flux near plant tissues using a self-referencing optrode. *Methods in Molecular Biology*, 1670, 267–281.

Mugnai, S., Azzarello, E., Baluška, F. & Mancuso, S. (2012) Local root apex hypoxia induces NO-mediated hypoxic acclimation of the entire root. *Plant & Cell Physiology*, 53, 912–910.

Nelson, B.K., Cai, X. & Nebenführ, A. (2007) A multicolored set of *in vivo* organelle markers for colocalization studies in arabidopsis and other plants. *Plant Journal*, 51, 1126–1136.

Newman, I.A. (2001) Ion transport in roots: measurement of fluxes using ion-selective microelectrodes to characterize transporter function. *Plant Cell & Environment*, 24, 1–14.

Norris, W.E., Jr., Harber, E.J. & Butler, J.E., III. (1959) Cellular respiration in onion root tips. *Botanical Gazette*, 120, 131–137.

Pandolfi, C., Mugnai, S., Azzarello, E., Masi, E., Pollastri, S. & Mancuso, S. (2012) The vibrating probe technique in the study of root physiology under stress. In: Mancuso, S. (Ed.) *Measuring roots*. Berlin, Heidelberg: Springer, pp. 67–81.

Pang, J.Y., Newman, I., Mendham, N., Zhou, M. & Shabala, S. (2006) Microelectrode ion and O_2 fluxes measurements reveal differential sensitivity of barley root tissues to hypoxia. *Plant Cell & Environment*, 29, 1107–1121.

Patel, D., Basu, M., Hayes, S., Majath, I., Hetherington, F.M., Tschaplinski, T.J. et al. (2013) Temperature-dependent shade avoidance involves the receptor-like kinase ERECTA. *Plant Journal*, 73, 980–992.

Parent, B. & Tardieu, F. (2012) Temperature responses of developmental processes have not been affected by breeding in different ecological areas for 17 crop species. *New Phytologist*, 194, 760–774.

Pernisova, M., Prat, T., Grones, P., Harustiakova, D., Matonohova, M., Spichal, L. et al. (2016) Cytokinins influence root gravitropism via differential regulation of auxin transporter expression and localization in arabidopsis. *New Phytologist*, 212, 497–509.

Peters, W.S. & Baskin, T.I. (2006) Tailor-made composite functions as tools in model choice: the case of sigmoidal vs bi-linear growth profiles. *Plant Methods*, 2, 12.

Poorter, H., Remkes, C. & Lambers, H. (1990) Carbon and nitrogen economy of 24 wild species differing in relative growth rate. *Plant Physiology*, 94, 621–627.

Poorter, H., van der Werf, A., Atkin, O.K. & Lambers, H. (1991) Respiratory energy requirements of roots vary with the potential growth rate of a plant species. *Physiologia Plantarum*, 83, 469–475.

Qi, Y., Xu, Y., Huang, H., Sun, Y. & Xu, L. (2004) ERECTA is required for protection against heat-stress in the AS1/AS2 pathway to regulate adaxial-abaxial leaf polarity in arabidopsis. *Planta*, 219, 270–276.

Riefler, M., Novak, O., Strnad, M. & Schmülling, T. (2006) Arabidopsis cytokinin receptor mutants reveal functions in shoot growth, leaf senescence, seed size, germination, root development, and cytokinin metabolism. *Plant Cell*, 18, 40–54.

Ross-Elliott, T.J., Jensen, K.H., Haaning, K.S., Wager, B.M., Knoblauch, J., Howell, A.H. et al. (2017) Phloem unloading in arabidopsis roots is convective and regulated by the phloem-pole pericycle. *eLife*, 6, e24125. https://doi.org/10.7554/eLife.24125.001

Rumman, M., Dhawan, J. & Kassem, M. (2015) Quiescence in adult stem cells: biological significance and relevance to tissue regeneration. *Stem Cells*, 33, 2903–2912.

Scafaro, A.P., Fan, Y., Posch, B.C., Garcia, A., Coast, O. & Atkin, O.K. (2021) Responses of leaf respiration to heatwaves. *Plant Cell & Environment*, 44, 2090–2101.

Schaller, G.E., Bishopp, A. & Kieber, J.J. (2015) The yin-yang of hormones: cytokinin and auxin interactions in plant development. *Plant Cell*, 27, 44–63.

Scheurwater, I., Cornelissen, C., Dictus, F., Welschen, R. & Lambers, H. (1998) Why do fast- and slow-growing grass species differ so little in their rate of root respiration, considering the large differences in rate of growth and ion uptake? *Plant Cell & Environment*, 21, 995–1005.

Schlesinger, W.H. (1997) *Biogeochemsitry. An analysis of global change*. San Diego, CA: Academic Press.

Schneider, C.A., Rasband, W.S. & Eliceiri, K.W. (2012) NIH image to ImageJ: 25 years of image analysis. *Nature Methods*, 9, 671–675.

Shen, H., Zhong, X., Zhao, F., Wang, Y., Yan, B., Li, Q. et al. (2015) Overexpression of receptor-like kinase ERECTA improves thermotolerance in rice and tomato. *Nature Biotechnology*, 33, 996–1003.

Silk, W.K. (1984) Quantitative descriptions of development. *Annual Review of Plant Physiology and Plant Molecular Biology*, 35, 479–518.

Silk, W.K. (1992) Steady form from changing cells. *International Journal of Plant Sciences*, 153, s49–s58.

Silk, W.K., Lord, E.M. & Eckard, K.J. (1989) Growth patterns inferred from anatomical records. Empirical tests using longisections of roots of *Zea mays* L. *Plant Physiology*, 90, 708–713.

Stepniewski, W., Zausig, J., Przywara, G. & Horn, R. (1998) Oxygen concentration in primary roots of broadbean, lupin and pea seedlings as measured with a microelectrode. *International Agrophysics*, 12, 87–95.

Tcherkez, G., Boex-Fontvieille, E., Mahé, A. & Hodge, M. (2012) Respiratory carbon flexes in leaves. *Current Opinion in Plant Biology*, 15, 308–314.

Torii, K.U., Mitsukawa, N., Oosumi, T., Matsuura, Y., Yokoyama, R., Whittier, R.F. et al. (1996) The arabidopsis *ERECTA* gene encodes a putative receptor protein kinase with extracellular leucine-rich repeats. *Plant Cell*, 8, 735–746.

van Aardt, W.J., le Roux, J.M., Lindeque, J.Z., Mason, S. & Louw, R. (2016) The effect of temperature on the respiration and metabolism of the African burrowing scorpion (*Opistophthalmus latimanus*). *Comparative Biochemistry & Physiology-Part D: Genomics & Proteomics*, 20, 50–56.

van der Werf, A., Kooijman, W.R. & Lambers, H. (1988) Respiratory energy costs for the maintenance of biomass, for growth and for ion uptake in roots of *Carex diandra* and *Carex acutiformis*. *Physiologia Plantarum*, 72, 483–491.

Vives-Peris, V., de Ollas, C., Gómez-Cadenas, A. & Pérez-Clemente, R.M. (2020) Root exudates: from plant to rhizosphere and beyond. *Plant Cell Reports*, 39, 3–17.

Weits, D.A., van Dongen, J.T. & Licausi, F. (2021) Molecular oxygen as a signaling component in plant development. *New Phytologist*, 229, 24–35.

Wu, Y., Spollen, W.G., Sharp, R.E., Hetherington, p.R. & Fry, S.C. (1994) Root growth maintenance at low water potentials. Increased activity of xyloglucan endotransglycosylase and its possible regulation by abscisic acid. *Plant Physiology*, 106, 607–615.

Xiao, Z., Rogiers, S., Sadras, V. & Tyerman, S. (2018) Hypoxia in grape berries: the role of seed respiration and lenticels on the berry pedicel and the possible link to cell death. *Journal of Experimental Botany*, 69, 2071–2083.

Yang, X., Dong, G., Palaniappan, K., Mi, G. & Baskin, T.I. (2017) Temperature-compensated cell production rate and elongation zone length in the root of *Arabidopsis thaliana*. *Plant, Cell & Environment*, 40, 264–276.

Zwiazek, J.J., Xu, H., Tan, X., Navarro-Ródenas, A. & Morte, A. (2017) Significance of oxygen transport through aquaporins. *Scientific Reports*, 7, 40411.

How to cite this article: Zimmermann, M.J., Bose, J., Kramer, E.M., Atkin, O.K., Tyerman, S.D. & Baskin, T.I. (2022) Oxygen uptake rates have contrasting responses to temperature in the root meristem and elongation zone. *Physiologia Plantarum*, 174(2), e13682. Available from: https://doi.org/10.1111/ppl.13682